Reverse Monte Carlo analysis of the structure of glassy carbon using electron-microscopy data

B. O'Malley and I. Snook
Department of Applied Physics, RM.I.T., GPO Box 2476V, Melbourne, Victoria, Australia 3001

D. McCulloch
Electron Microscopy Unit, University of Sydney, Sydney, New South Wales, Australia 2006
(Received 8 July 1997)

The reverse Monte Carlo (RMC) method was utilized in order to obtain three-dimensional atom configurations in glassy carbon using measurements of the static structure provided by electron diffraction. This allowed the local and medium-range order in glassy carbon formed at heat-treatment temperatures of 1000 and 2500 °C to be analyzed in detail. In particular, the nature of the graphitelike bonding within the glassy-carbon structure was investigated as well as the form of disorder that gives rise to the particular features of its static structure factor. The configurations produced by the RMC method consisted of randomly stacked graphitic basal planes possessing a buckled nature. It was found that significant nongraphitic regions exist in glassy carbon including the presence of three- and five-membered rings. These disordered regions decrease in extent as the heat-treatment temperature increases. [S0163-1829(98)06022-6]

INTRODUCTION

In recent years several forms of crystalline and noncrystalline carbons have been discovered, testament to the wide range of chemical bonds that carbon can form. These include crystalline forms such as fullerenes and carbon nanotubes, and disordered forms such as glassy carbon and amorphous and diamondlike amorphous carbon. Glassy or vitreous carbon[1] belongs to a class of disordered, largely graphitic carbons that remain stable against graphitization to temperatures up to 3000 °C. It has a low density compared to graphite and along with other nongraphitizing carbons bears some resemblance to its precursor polymer. It is produced by pyrolysis of resins when heated to temperatures between 1000 and 2700 °C. The chemical inertness and high electrical conductivity of glassy carbon have led to its application in the manufacture of crucibles and electrodes.[1]

In this paper the structure of glassy carbon formed at heat-treatment temperatures of 1000 and 2500 °C (denoted as v10 and v25, respectively, in this paper) has been investigated in detail using the reverse Monte Carlo (RMC) method. The experimental structure factor of the different forms of glassy carbon was obtained using electron diffraction in a transmission electron microscope (TEM). This study of glassy carbon formed at different temperatures is motivated by the differences in their structure apparent from high-resolution TEM images (see Fig. 1). In addition, although several structural models have been proposed, the exact structural arrangements present in glassy carbon are not well understood.

Apart from their technological importance, disordered carbons are examples of glasses with significant constraints on their possible structural topology due to the strong covalent bonding in carbon. A detailed analysis of the structure that exists in these materials is thus beneficial in developing general models of network glasses. In this regard, our work complements the considerably more extensive research on modeling the structure of silicate glasses.[2] Also the porous structure of glassy carbon makes it an interesting one-component model system for porous solids.

Structure of glassy carbon

On the basis of high-resolution TEM and diffraction studies it has been proposed that the microstructure of glassy carbon consists of a network of graphitelike ribbons containing many micropores.[1] The ribbons correspond to the largely sp^2-bonded basal planes that are randomly stacked on top of each other in bundles or fibers of up to 30 Å in width and 100 Å in length. These ribbons are thought to join in one of

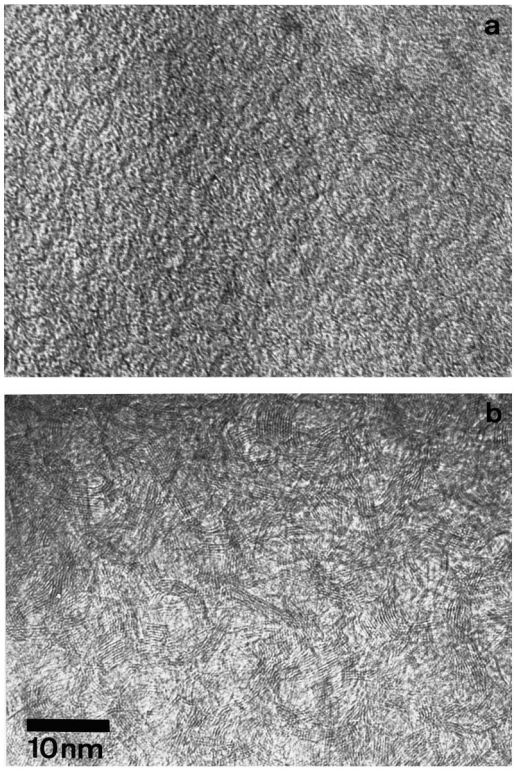

FIG. 1. High-resolution TEM image of v10 (a) and v25 (b) glassy carbon samples. The fringes observed are at a spacing of approximately 3.35 Å. Note that both (a) and (b) are at the same magnification.

two ways, either by the overlap of ribbons from different fibers or by the merger of the basal planes of different fibers. The presence of pores in the network explains the low density of glassy carbon. The diffraction pattern of glassy carbon reveals that the most intense reflection is that due to the (002) reflection, attributed to scattering from the basal planes of graphite. The absence of the intense (101) reflection observed in graphite and other $(h01)$ reflections in the diffraction pattern of glassy carbon is attributed to the lack of correct *ABA* stacking of the graphitic ribbons. The difference between the two samples examined in this paper is most easily observed by high-resolution TEM for which it can be seen that the ribbons lengthen considerably as the heat-treatment temperature is increased, as shown in Fig. 1.

Reverse Monte Carlo method

The RMC algorithm has been described in detail elsewhere;[3–5] in essence it is a computer simulation method for producing a set of particle configurations that is consistent with an input experimental static structure factor $S(q)$. The resulting configurations can then be subjected to various geometrical analyses to reveal information about the short- and intermediate-range order of the studied material that cannot be obtained directly from the $S(q)$ of a disordered material.

The RMC method is a very general method of reproducing the detailed structure of a material based only on the experimental diffraction data. No assumptions concerning the form of interatomic potential are necessary, which distinguishes this approach from conventional computer simulation methods such as molecular-dynamics simulations.[6]

The algorithm used in the RMC method is a variation of the metropolis Monte Carlo method for the calculation of ensemble averages of thermodynamic properties of a system of molecules, e.g., pressure or internal energy.[6] In a Monte Carlo simulation, configurations are chosen so as to produce a set of configurations with a Boltzmann distribution of energies. In RMC simulations, the difference between the experimental and calculated $S(q)$ is the quantity to be minimized χ^2, which is given by

$$\chi_c^2=\sum_{i=1}^{N_{\rm exp}} \frac{[S(q_i)_c-S(q_i)_{\rm exp}]^2}{\sigma_{\rm exp}(q_i)^2}, \tag{1}$$

where the subscripts c and exp refer to the static structure factor from the RMC configurations and experiment, respectively. $N_{\rm exp}$ is the number of experimental data points and $\sigma_{\rm exp}$ is an estimate of the experimental error.

The simulation starts with an appropriate initial configuration of atoms. An atom is randomly selected and moved a random distance. The new $S(q)$ of the configuration of atoms is calculated as well as χ^2. If the new error $\chi^2_{\rm new}$ is less than the old error $\chi^2_{\rm old}$, i.e., the agreement between the experimental and configuration $S(q)$ is improved by the move, then the move is accepted and another move made. If the error is increased by the move, it is not rejected outright but accepted with a probability $\exp[-(\chi^2_{\rm new}-\chi^2_{\rm old})/2]$. The process is then repeated until χ^2 oscillates about an equilibrium value. This method of minimizing the difference between the experimental $S(q)$ and one calculated from a three dimensionally generated structure ensures that the process is unlikely to get trapped into a local minima or is overly dependent on the initial choice of starting configuration.

A number of variations of the basic algorithm are possible. If it is known that a certain form of bonding exists in the material, e.g., a predominance of sp^2 bonding in the case of glassy carbon, then a ''coordination constraint'' can be employed in the simulation to only generate configurations for which the atoms have the desired bonding. In this case a coordination number is set for the atoms as well as the required fraction of atoms with this given coordination, e.g., in glassy carbon every carbon atom has three nearest neighbors corresponding to 100% sp^2 bonding. An additional term is also added to the above error term,

$$\chi_c^2=\frac{(f_{\rm RMC}-f_{\rm req})^2}{w_c^2}, \tag{2}$$

where $f_{\rm req}$ is the required fraction of properly coordinated atoms, $f_{\rm RMC}$ is the fraction of atoms in the configuration with the proper coordination, and w_c is a weighting factor. If w_c is very small and $f_{\rm req}$ set to 1 then most moves that ''break'' the bonds will be rejected. Thus models of the structure of a material can be produced with a specified form of bonding or type of molecular unit.

The structures obtained from the RMC method are not unique due to the limited, two-body nature of the information contained in the input structure factor. Thus a number of possible structural configurations can be fitted to the $S(q)$ data alone. In dense systems, packing constraints are expected to strongly influence the structure and the variety of generated structures will be limited by the hard-core diameter of the atoms. On the other hand, for low-density materials, such as glassy carbon, packing constraints will not play a significant role and the coordination constraints described above are necessary in order to generate reasonable structures. A reasonable choice of staring configuration is also required, in order to limit the search of configuration space to likely candidate structures.

CALCULATION DETAILS

It is known from electron-energy-loss spectroscopy that glassy carbon is nearly 100% sp^2 bonded.[7] Hence a perfect graphite crystal was chosen as the starting configuration for the RMC simulations started with a graphite crystal and moves that decreased the coordination number from the graphite value of 3 were weighted against using a coordination constraint, as described above.

The number density used in this work is that of crystalline graphite, 2.27 g/cm^3, rather than the much lower density of glassy carbon. The reason for using this density is that the information contained in the $S(q)$ pertains to the scattering from the graphiticlike ribbons not the micropores. Hence this work is only concerned with the structure within the graphitelike ribbons rather than the overall arrangement of the ribbons in space. Jenkins and Kawamura[8] have estimated the average pore size of glassy carbon as between 50–100 Å. In order to model the ribbon structure and pore network together, scattering data on this length scale would be required, e.g., from low-angle x-ray scattering.

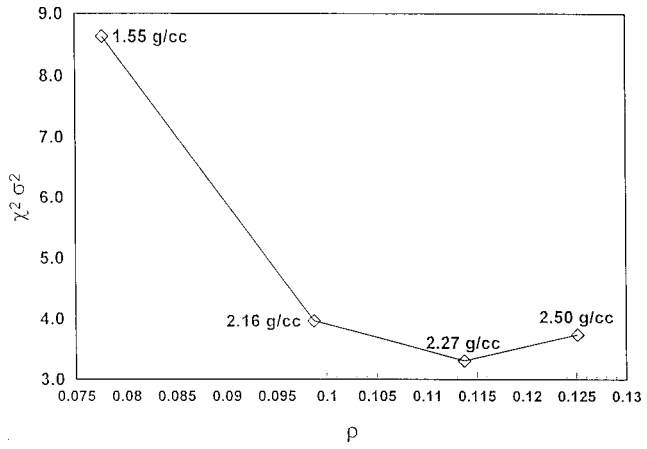

FIG. 2. Equilibrium value of χ^2 as a function of input number density. The horizontal axis is in units of atoms/Å^3.

In order to test the validity of assuming a number density equal to that of crystalline graphite a number of RMC calculations were performed using different input number densities to model the $S(q)$ of our v10 sample. The motivation for this approach is based on the observation that χ^2 has its minimum value at the correct number density of the modeled material.[9]

The first density used was that of crystalline graphite, 2.27 g/cm^3. The second density corresponded to the actual density of glassy carbon, 1.55 g/cm^3; the third was derived from the position of the (002) peak in the $S(q)$ of the v25 sample of glassy carbon, 2.16 g/cm^3; and the fourth was at a density 10% greater than the crystalline graphite, 2.50 g/cm^3. The value of the third density is based on assuming that the number density of the basal planes is unchanged in glassy carbon as compared to graphite and the peak position q_{002} can be used to estimate the average distance separating the basal planes where c-axis distance is $2\pi/q_{002}$.

It can be seen in Fig. 2 that χ^2 has a minimum value at the number density of crystalline graphite. The stored configurations from the RMC simulation at the glassy carbon number density were also analyzed. A highly disconnected network was observed with no graphitic nature and many nonbonded carbon atoms.

The RMC simulations contained 7776 atoms with a starting configuration and the density of crystalline graphite. The starting configuration was a graphite crystal. A minimum distance of approach of 0.85 Å was used. A maximum C-C bond length of 1.91 Å was used. This distance is equal to the first minimum in the experimental pair-correlation function.

The value of w_c used in this work was 0.0001. This enabled the data to be fitted accurately while maintaining the sp^2 coordination of most (99.2%) carbon atoms. The appropriateness of this value was tested by performing RMC calculations with two other values, 0.01 and 0.000 01. In the former case the fit to the experimental $S(q)$ was approximately the same, but the fraction of sp^2 atoms after equilibration was only 47%. In the latter case the fit to the data was marginally worse and the percentage of sp^2 coordinated atoms increased to 99.8%. These results reflect the competition between the two error terms in the acceptance condition, the first measuring the fit to the data and the second the sp^2 coordination. A large value of w_c allows atom moves that improve the fit to the experimental data to be accepted, even if the coordination number changes from sp^2, while a small value predominantly allows only moves that leave the original sp^2 coordination unchanged.

Glassy-carbon specimens heat treated to 1000 and 2500 °C were purchased in plate form from Atomergic Chemetals Corporation (New York). According to the manufacturer's specifications, the density of the material was 1.5–1.55 g/cm^3. Specimens suitably thin for TEM were prepared using ultramicrotomy. The specimens were then placed in a Philips 430 TEM operating at 300 kV. Energy-filtered electron-diffraction patterns were then collected by scanning the diffraction pattern of each specimen over the entrance aperture of a Gatan 666 parallel electron-energy-loss spectrometer as described elsewhere.[10] The static structure factor $S(q)$ was then determined by

$$S(q)=\frac{I(q)-Nf^2}{Nf^2}\,\frac{2\pi}{q}+1, \tag{3}$$

where $I(q)$ is the elastic scattered intensity, f is the atomic scattering amplitude, and N is a scaling factor.[11] The normalizing factor N is obtained by choosing the value of N that gives the best fit between Nf^2 and $I(q)$ at high q. N is loosely related to the number of atoms in the beam.

RESULTS

Structure factor and pair-correlation function

The experimental static structure factor $S(q)$ and pair-correlation function $g(r)$ for the v10 and v25 samples, as well as the RMC results are shown in Figs. 3 and 4. The agreement between the structure factors is good with significant deviations only at low q. Details can be found in Table I.

The differences between the experimental and RMC $S(q)$ at low q are to be expected due to the enhancement of uncertainties in the data in this wave-vector range $q<5.00$ Å^{-1}. The experimental $g(r)$ exhibits a large negative dip at low r, which is normally a sign of systematic errors in $S(q)$.[12] In order to obtain an estimate of the best possible agreement between the RMC and experimental $S(q)$'s, the experimental $g(r)$ for the v25 sample was set to zero for r less than the hard core diameter and then Fourier transformed to $S(q)$. It is found that the deviations in the resulting $S(q)$ follow the observed deviations between the RMC $S(q)$ and the experimental $S(q)$ at low q. Differences in the experimentally and RMC generated fit to $g(r)$ are small for both samples, with the heights of the first few peaks in the RMC $g(r)$ fits slightly lower than the experimental data.

Nearest-neighbor distribution

The local order in glassy carbon was analyzed by calculating the distribution of coordination numbers for the first three neighbor shells and the distribution of bond angles within the first neighbor shell. The radii of the ith neighbor shell was set equal to the value of r_i for the ith minima in the radial distribution function $g(r_i)$. The radii were the same for both samples and were set at 1.91, 2.74, and 3.28 Å, for the first, second, and third neighbor shells, respectively. The

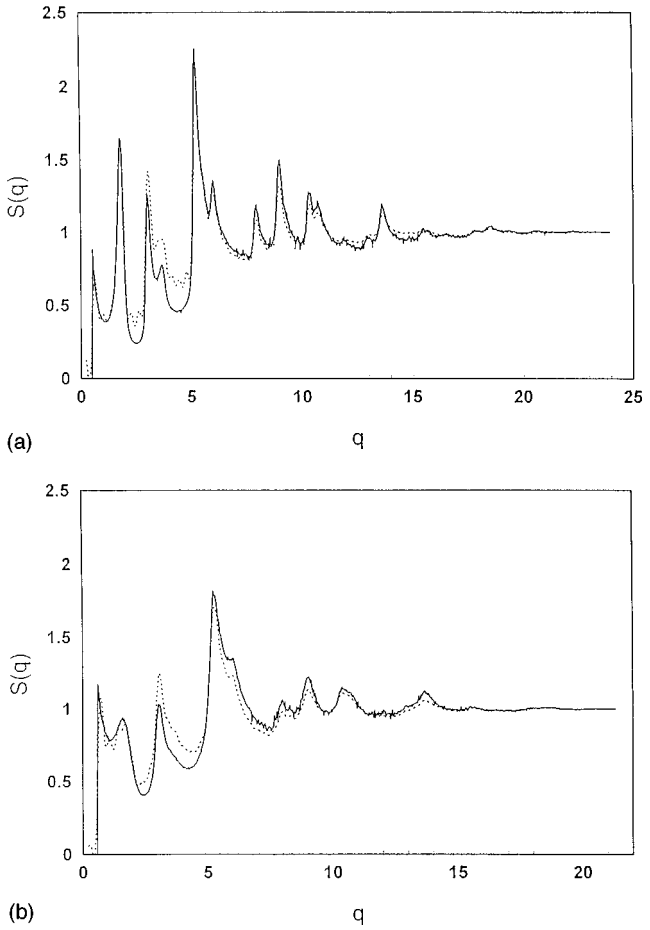

FIG. 3. Structure factors of glassy carbon samples (a) v25 and (b) v10. ——, experimental data; ---------, RMC modeling of $S(q)$. The horizontal axis is in units of Å^{-1}.

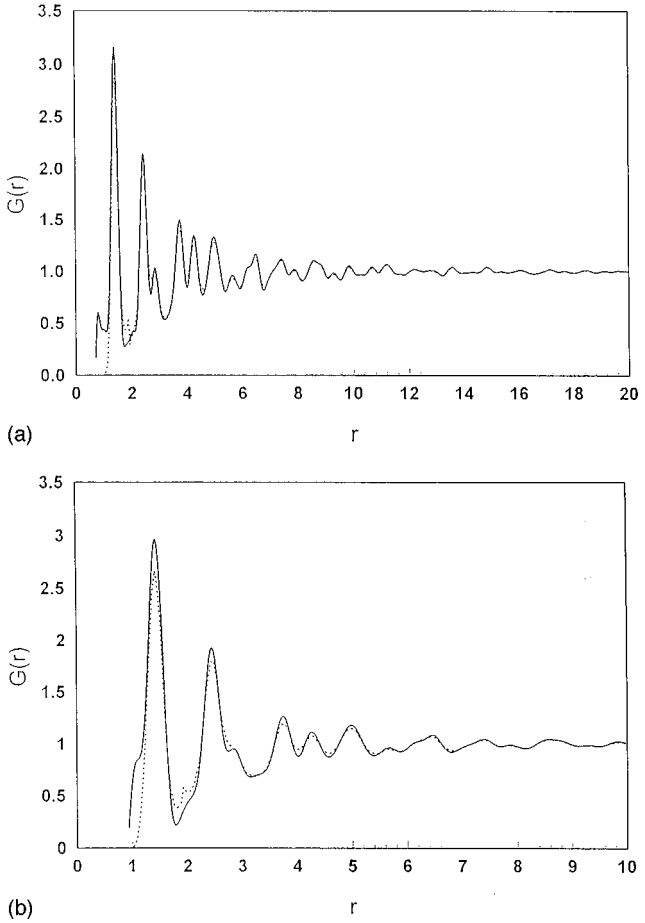

FIG. 4. Pair-correlation functions of glassy carbon samples (a) v25 and (b) v10. ——, experimental data; ---------, RMC modeling of $S(q)$. The horizontal axis is in units of Å.

resulting broad distribution of nearest neighbors is similar for both samples and is displayed in Fig. 5.

The most obvious feature of these distributions is the skew towards higher coordination numbers, which is more pronounced in the case of the v10 sample. The second-nearest-neighbor distribution is peaked at a coordination number of 7 for the v10 sample and 6 for the v25 sample, and the third-nearest-neighbor distributions are peaked at coordination numbers of 6 and 5 for the v10 and v25 samples, respectively. In comparison, graphite possesses 6 second-nearest neighbors and 3 third-nearest neighbors for the same neighbor-shell radii. These neighbors are within the same basal plane in graphite at distances of 1.42, 2.46, and 2.84 Å, respectively. The value of the coordination numbers for the second-nearest-neighbor shell is in good agreement with that to be expected from a disordered graphite network, although the broadness of the distributions is surprising. We will return to this point later. The large peak coordination number in the third shell is obviously due to a considerable inclusion of extra third-nearest neighbors that are not of the kind observed in graphite.

Bond-angle distribution

The bond-angle distribution of both samples of glassy carbon is shown in Fig. 6. It is peaked at a bond angle of approximately 117° for both samples, slightly less than the ideal graphitic bond angle of 120°. The peak height is slightly larger in the v25 sample than the v10 sample. The distribution of bond angles is broad in both samples and is skewed towards lower angles with a very small peak at approximately 60°. The standard deviation of the bond-angle distribution for both samples is equal to approximately 18°. The increased broadness in the bond-angle distribution for the v10 sample is most noticeable for large bond angles, i.e., greater than 117°. These small differences indicate that the v10 sample may be slightly more disordered on an atomic length scale, but given the $S(q)$'s for both samples are not fitted perfectly, care should be taken in regarding the differences as significant.

Network-neighbor distribution

A network definition of nearest neighbors was also used to calculate alternative neighbor distributions. An atom is

TABLE I. Details of simulation results. N_{exp} is the number of data points fitted in the experimental $S(q)$.

Sample	$\chi^2 * \sigma_{\text{exp}}{}^2 N_{\text{exp}}$	% of sp^2 atoms
v10	0.0049	99.3
v25	0.0065	99.2

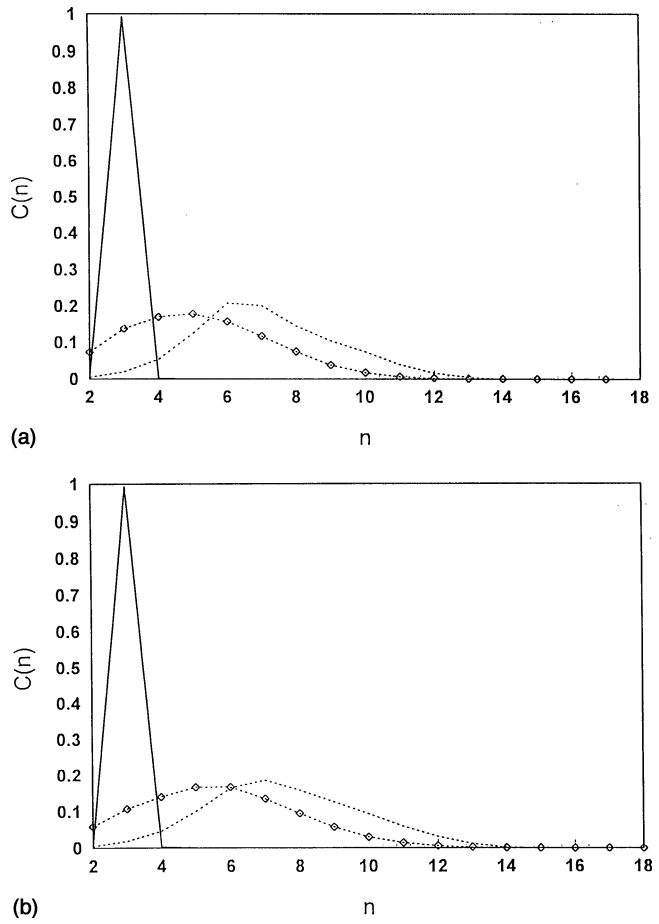

FIG. 5. Neighbor distributions for first three neighbor shells of (a) v25 and (b) v10 sample. ——, nearest neighbors; ---------, second nearest neighbors; -◇-◇-, third-nearest-neighbor distribution.

regarded as an ith-nearest neighbor of another atom if and only if the shortest path joining the two atoms via the network of bonds involves i bonds. The normalized fraction of atoms with the same number n of ith nearest neighbors as graphite $C(n,i)$ is given in Table II up to fourth ''nearest neighbors.''

The neighbor distributions are sharply peaked at the coordination numbers expected for a perfect graphite crystal. Significant deviations only occur beyond the third-nearest-neighbor shell. Hence the short- and medium-range order of the two glassy carbon samples possesses a connectivity very similar to that of graphite, deviations from a graphite network being more noticeable in the case of the v10 sample. This result is supported by electron-energy-loss carbon k-edge measurements of glassy carbon and crystalline graphite that show very similar near-edge fine structure indicating that both contain similar local atomic environments.[7]

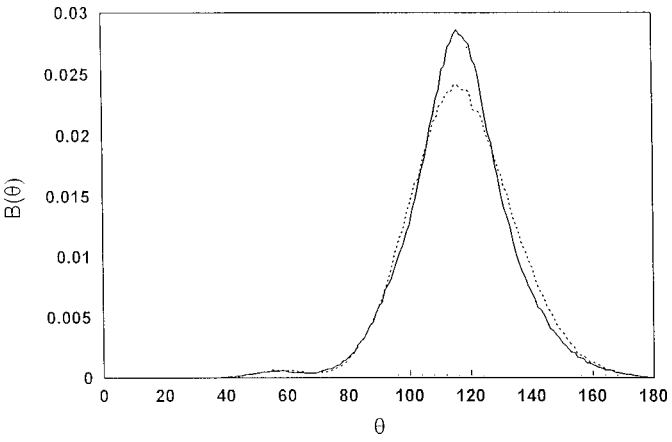

FIG. 6. Bond-angle distribution. ——, v25 sample; ---------, v10 sample.

TABLE II. Normalized fraction of atoms with the same ith nearest-neighbor coordination as in graphite. Graphite has 3 nearest neighbors, 6 second nearest neighbors, 9 third nearest neighbors, and 12 fourth nearest neighbors for the network-neighbor definition.

Sample	C(3,1)	C(6,2)	C(9,3)	C(12,4)
v25	0.992	0.938	0.812	0.744
v10	0.993	0.934	0.791	0.727

The pair-correlation function can also be decomposed into a contribution from the different neighbor shells, denoted as $g_N(r)$, and is shown in Fig. 7 for the v25 sample and Fig. 8 for the v10 sample. It can be seen that the neighbor $g_N(r)$'s are broader in the case of the v10 sample.

It can be seen from Fig. 7 that the neighbor $g_N(r)$'s do not sum up to the total $g(r)$ for this system. In the case of a fully connected network of atoms it would be expected that the $g_N(r)$'s do add up to the total $g(r)$ and this has been successfully tested for a soft-sphere liquid system. The reason this is not the case for our glassy carbon model is that there are very few bonds between neighboring basal planes and hence atom pairs in different basal planes that contribute to the total $g(r)$ will not contribute to the network $g(r)$'s as there is no sequence of bonds connecting these pairs in general. Thus these $g_N(r)$'s predominantly reveal information about the structure of the basal planes. Also, the difference between the total $g(r)$ and the sum of the network $g(r)$'s gives an indication of the contribution of intraplanar distances to the total $g(r)$.

The connectivity of the two samples is similar and highly graphitic in nature but the possible distances of neighbors is broader for the v10 sample. A small shoulder in the third-

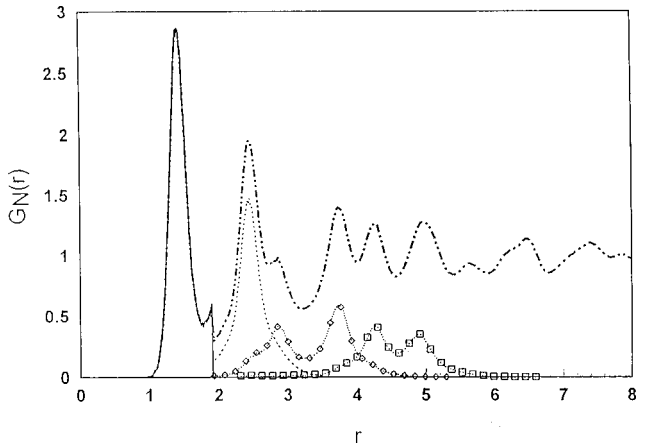

FIG. 7. Pair-correlation function decomposed into contributions from different neighbor shells for the v25 sample. ——, first shell; ---------, second shell;-◇-◇-, third shell; -□-□-, fourth shell. The horizontal axis is in units of Å.

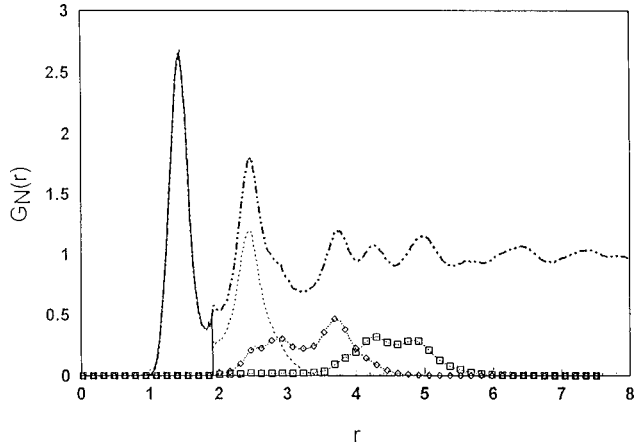

FIG. 8. Pair-correlation function decomposed into contributions from different neighbor shells for the v10 sample. ——, first shell; ---------, second shell; -◇-◇-, third shell; -□-□-line, fourth shell. The horizontal axis is in units of Å.

network-neighbor $g_N(r)$ at approximately 2.45 Å indicates that some third network nearest neighbors are at second-nearest-neighbor distances indicating that there is significant distortion of the hexagonal rings forming the graphitic network. This would also account for the broadness of the conventionally defined nearest-neighbor distributions due to the considerable overlap of the second and third peaks in the $g(r)$ of the glassy carbon samples.

Computer visualization

A computer visualization of the stored configurations reveals that the simulated structure consists of graphiticlike basal planes randomly stacked in the c-axis direction. Figure 9(a) shows a typical basal plane from the stored configurations from the modeled v10 sample, a slice parallel to the c-axis direction and 3.35 Å thick. The v25 sample has a similar appearance. The basal planes or ribbons are nonplanar exhibiting a buckled form. It can be observed in Fig. 9(a) that there are a number of large rings or ''holes'' in the graphite network. This is a common feature of all planes observed, and many of the non-six-membered rings cluster around these features. In Fig. 9(b) a side-on view of the same plane reveals the buckled nature of the basal planes. The combination of the random stacking of the basal planes and their buckling can be considered sufficient to destroy any interplanar register and thus no $(h01)$ reflections will be observed.

The broad range of coordination numbers using the radii shell definition can be attributed to the nonplanar form of the ribbons. For a set radius, the effect of buckling a perfect planar graphite structure will be to increase the average coordination number. Combined with the observed holes, for which the coordination number will be reduced, this leads to the broad nearest-neighbor distributions.

The lightly shaded atoms in Fig. 9 are atoms that are in a disordered region. An atom is regarded as in an ordered local neighborhood if three hexagonal rings pass through the atom as in graphite. All other atoms are regarded as being in a disordered neighborhood. These disordered regions are characterized by pairs of three- and five-membered rings and the previously mentioned large holes. These observations will be discussed later in more detail.

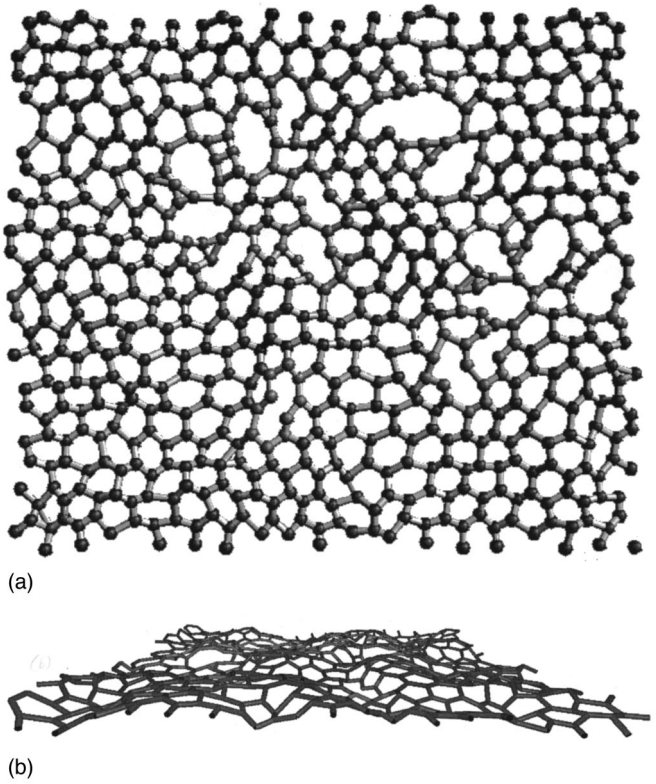

FIG. 9. (a) A basal plane from the stored RMC configurations for the v10 sample viewed down the direction of stacking, i.e., the c-axis direction. The lightly shaded atoms are in a disordered region. (b) A side on view of the same basal plane as in (a).

Buckling of basal planes

The buckled nature of the basal planes was further investigated to elucidate whether this was a necessary feature for models of glassy carbon. An RMC simulation was performed using identical parameters as the previous simulation for the v25 sample but only allowing the atoms to disorder within the basal plane. It was found that there was a very poor level of agreement with the experimental $S(q)$ and hence we can conclude that basal plane disorder is insufficient to describe the structure of glassy carbon and the curvature of the basal planes is an integral feature of this material. It may seem obvious from any TEM image of glassy carbon that the ''ribbons'' are curved but the curvature of the ribbons appears in large part to be quite shallow with respect to the length scales discussed in this work. Hence our work demonstrates the importance of including the effects of locally strong curvature on any structural model of glassy carbon.

One of the most significant differences between the two samples is the height of the (002) peak, attributed to the stacking of graphitic basal planes. The density variation in the c-axis direction (the stacking direction of the basal planes) was investigated by calculating the pair-correlation function in this direction $g(z)$, which corresponds to the z-axis direction of our simulation cell. It is equal to the pair-correlation function averaged over the two other independent

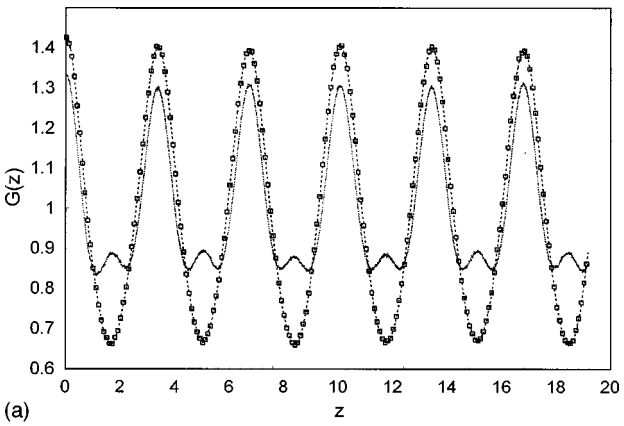

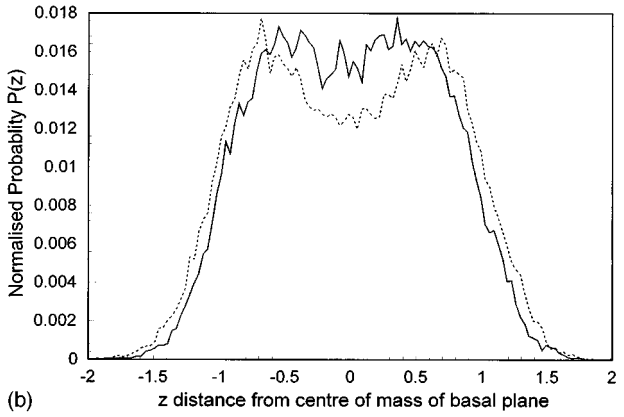

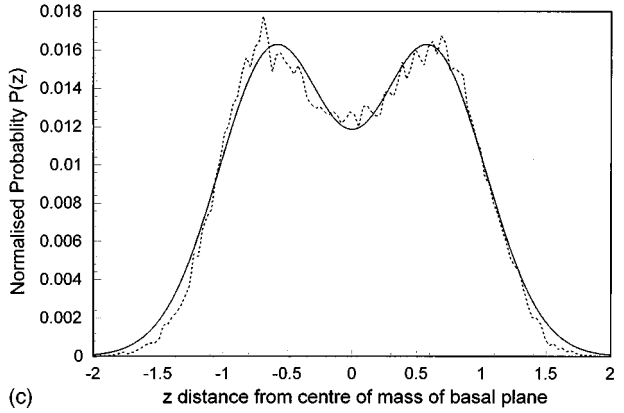

FIG. 10. (a) Reduced-pair correlation function $g(z)$. --□--□--, v25 sample; ---------, v10 sample. The horizontal axis is in units of Å. (b) Breadth distribution for basal planes. ——, v25 sample;---------, v10 sample. The horizontal axis is in units of Å. (c) Gaussian fit to breadth distribution for basal planes of v10 sample. ——, Gaussian fit; ---------, v10 breadth distribution. The horizontal axis is in units of Å.

directions in the simulation cell. For both samples the average spacing of the planes is 3.35 Å in the c-axis direction [Fig. 10(a)]. The $g(z)$ has a sinusoidal form with a period of 3.35 Å. The height of the peaks in the $g(z)$ for the v10 sample is significantly reduced compared to the v25 sample and there is a small maxima between the planes. This may indicate a degree of cross linking of the planes in the v10 sample, but a calculation of the number of atoms that are bonded to atoms in more than one plane does not justify this assertion; the fraction of such atoms is very small ($<0.1\%$) and similar for both samples. The nonplanar nature of the basal planes is clearly indicated by these results, as well as the fact that the buckling of the basal planes is greater in the v10 sample.

TABLE III. Values of parameters used to fit breadth distributions to a double Gaussian, Eq. (4).

Sample	A	μ	σ	d
v10	0.016	−0.60	0.60	1.20
v25	0.016	−0.53	0.60	1.04

The breadth of the basal planes was also calculated. In order to achieve this, each atom was assigned to a given plane based on its z position. In the case of ambiguity, where an atom position is in the minima between two planes, the atom is assigned to the plane in which a dominant number of its nearest neighbors reside. The mean position of each plane was then calculated. Using this mean position, the distribution of the z component of the positions of the atoms in the plane about the mean position was calculated. This distribution was averaged over each plane and stored configuration. The breadth distributions for both samples are double peaked. This clearly reflects the buckling of the planes; most atoms lie in planes above or below the center plane. The distributions for both samples can be fitted to a double Gaussian of the form

$$b(z)=Ae^{[(\mu-z)/\sigma]^2}+Ae^{-[(\mu+d-z)/\sigma]^2}, \tag{4}$$

where d is the distance between the peak positions of the Gaussians. A fit to both distributions reveals that the difference between the distributions is a decreased separation of the two Gaussians for the v25 sample (d) with respect to the v10 sample, while the variance and height for both samples have nearly identical values. The values used in the fits for both samples are given in Table III. We can conclude from these results that the amplitude of the buckling is greater in the v10 sample. These results are consistent with a general picture of the difference between the samples being the degree of curvature of the basal planes.

Ring statistics

In order to investigate the medium-range structure of glassy carbon, ring statistics were calculated for the stored RMC configurations, where the definition of a ring is given by the shortest path criterion of Franzblau.[13] Shortest path rings are restricted to those rings forming closed paths such that for every pair of vertices of the ring the shortest path around the network is around the ring. This definition avoids the counting of compound rings formed by two intersecting rings but is not simply restricted to counting only the shortest rings in the network.

The average number of rings passing through the atoms as a function of ring size is given in Table IV. The total number of rings of each type is given in Table V. The dominant contribution is from six-membered rings emphasizing again the graphitic nature of glassy carbon. A small number of rings of other sizes were also found. The number of nonhexagonal rings was greater in the v10 sample.

The bond angles between neighboring atoms in a ring were also calculated and are displayed in Fig. 11 for the most

TABLE IV. Average number of rings of size R passing through each atom $N(R)$. The total number of rings of a given size R in the simulated structure is equal to $N(R)/R$ (number of atoms equals 7776); the factor R in the denominator is to avoid counting the rings more than once.

Sample	$N(3)$	$N(4)$	$N(5)$	$N(6)$	$N(7)$	$N(8)$	$N(9)$
v25	0.039	0.004	0.048	2.67	0.013	0.004	0.032
v10	0.045	0.013	0.053	2.63	0.011	0.020	0.038
graphite	⋯	⋯	⋯	3.00	⋯	⋯	⋯

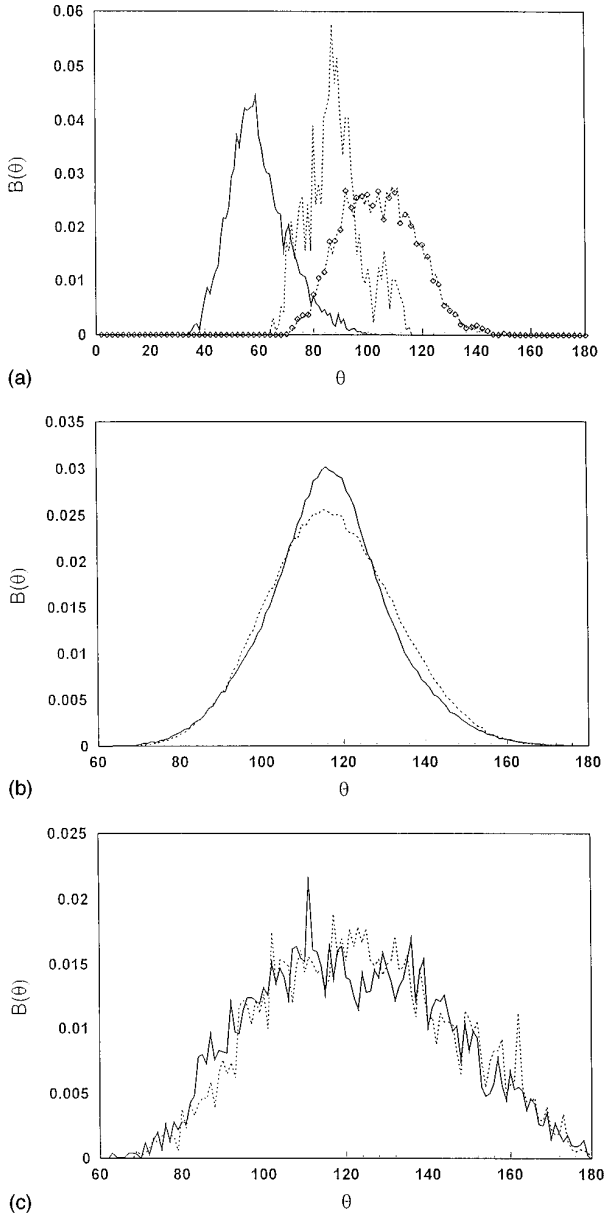

FIG. 11. (a) Normalized bond-angle distribution for the bond angles between neighboring atoms in a ring for the v25 sample. ——, 3-membered rings; ---------, 4-membered rings; -◇-◇-, 5-membered rings. (b) Comparison of normalized bond-angle distribution for the bond angles between neighboring atoms of the 6-membered rings. ——, v25; ---------, v10. (c) Comparison of normalized bond-angle distribution for the bond angles between neighboring atoms of the 9-membered rings. ——, v25; ---------, v10.

common rings. The bond-angle distributions for the three-, five-, and nine-membered rings for the v10 and v25 sample are identical. These rings are the most common after the dominant six-membered rings. Significant differences between the samples only appear in the bond-angle distribution for the six-membered rings.

The skew in the total bond-angle distribution at small angles was found to be due to the presence of four- and five-membered rings with average bond angles of 91° and 105°, respectively. The average bond angle for the nine-membered rings was 121° and possessed a broad distribution with a standard deviation of 22°. The small peak at 60° in the total bond-angle distribution is due to the presence of three-membered rings. The average bond angle for the six-membered rings was equal to 117° for both samples. This indicates that the peak in the total bond-angle distribution at 117° is a feature of the dominant six-membered rings while the broadness of the distribution is in part due to rings of other sizes. The peak height for the bond-angle distribution of the six-membered rings was larger and the distribution narrower for the v25 sample.

The presence of a significant number of three-membered rings and a lesser number of four-membered rings is an interesting result of this work. Although it may be argued that these structures would be too strained to be stable, *ab initio* and tight-binding molecular-dynamics simulations of amorphous carbon have also revealed the presence of three- and four-membered rings in their simulated structures.[14,15] This work can be regarded as complementary to that but that in which the small rings appear as a necessary structural feature in order to create a three-dimensional model of glassy carbon consistent with the diffraction data.

The other most common nonhexagonal rings are five-membered rings. The existence of these rings is less contentious as they are observed in fullerene forms of carbon. They can be attributed to positive curvature in the basal planes as is the case for fullerenes.

A number of models of negatively curved graphitic carbon have been proposed that are commonly produced by the introduction of seven-membered or larger rings.[16] These rings can maintain bond angles of 120°, unlike five-membered rings, and hence strains on the structure are mini-

TABLE V. Total number of rings of for v25 sample, using data in Table III.

Ring size	3	4	5	6	7	8	9
Total	101	8	75	3460	14	4	28

TABLE VI. Most common ring sequences observed. P_{seqn}(RS) is the percentage of atoms that possess a ring sequence RS. Labeling system is of the form $(a,b,c,d\ldots)$, where a is the number of three-membered rings passing through an atom, b the number of four-membered rings, and so on up to nine-membered rings.

Ring sequence	v25 P_{seqn}(RS) (%)	v10 P_{seqn}(RS) (%)
(0 0 0 3 0 0 0)	81.36	78.24
(0 0 0 2 0 0 0)	6.57	7.10
(0 0 0 1 0 0 0)	1.86	1.87
(0 0 1 1 0 0 0)	1.49	1.49
(1 0 1 0 0 0 0)	1.47	1.48
(0 0 1 2 0 0 0)	1.11	1.12
(0 0 0 2 0 0 1)	1.00	1.31

mized. This is well illustrated in our work if the average bond angles of the five- and nine-membered rings are compared. These ''Schwarzite'' forms of carbon are predominantly symmetric and porous structures that are remarkably stable with respect to graphite. Townsend *et al.*[17] have generated a number of models of amorphous carbon in which sp^2 coordination is maintained in regions of strong local curvature by the introduction of a nonhexagonal rings. A model in which a random surface is covered with a graphitelike carbon network in order to simulate a random pore geometry revealed the presence of many five-, seven-, eight-, and nine-membered rings. These results suggest that the large rings observed in our simulated structures are indicative of negative curvature in regions of the RMC-generated basal planes.

The value of 117° for the average bond angle in glassy carbon also appears in *ab initio* simulations of amorphous carbon.[18] Amorphous carbon is dominantly sp^2 bonded with the remaining atoms sp^3 bonded. It is thought to posses a mixed graphitic and diamondlike structure. Galli *et al.*[18] simulated an a-C structure that was 85% sp^2 bonded for which the average bond angle of sp^2 sites was 117°. The sp^2 regions were graphitic in nature tending to lie in buckled planes giving them a finite thickness of about 1 Å. Their results are consistent with our observations although the approaches are entirely different. This suggests that the slight reduction in the bond angle of the hexagonal rings may be a general feature of buckled graphitic planes.

Deviations from graphitic order were analyzed by labeling atoms depending on the type and number of rings of each type that they were members of and the results are given in Table VI. The most common sequence is that observed in graphite followed by sequences in which there is only a 1 or 2 hexagonal ring. If an atom has three nearest neighbors then we expect at least three rings would pass through the atom. Hence these ring sequences apply to atoms that are also on the edge of a large hole. As mentioned earlier, three- and five-membered ring pairs are common as well as pairs of five- and six-membered rings. It is interesting that there are a small number of atoms that are part of two six-membered rings and one five-membered ring. This is the same local environment of a carbon atom in C_{60}, i.e., fullerenes.

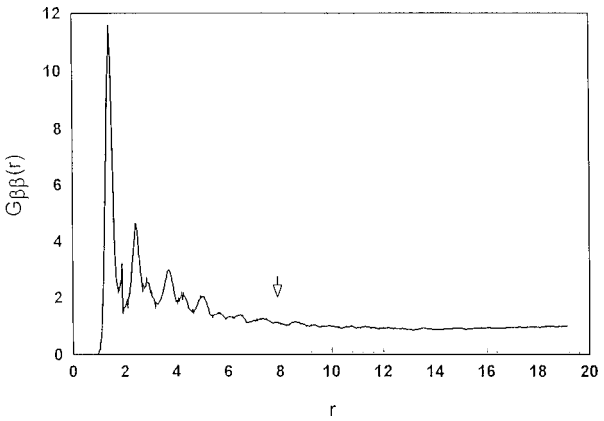

FIG. 12. Partial pair-correlation function for atoms in disordered regions $g_{\beta\beta}(r)$ for v25 sample. The arrow indicates the value of r at which $g_{\beta\beta}(r)$ first equals 1. The horizontal axis is in units of Å.

Clustering of defects

In order to investigate the influence of the nonhexagonal rings on the structure of glassy carbon, atoms were labeled as mentioned before as being either ordered or disordered. Denoting an atom as type α if it is in an ordered region and type β if it is not, the partial pair-correlation functions $g_{\alpha\alpha}(r)$, $g_{\alpha\beta}(r)$, and $g_{\beta\beta}(r)$ were calculated for both samples.

It can be seen in Fig. 12 that the partial $g(r)$ for the disordered atoms $g_{\beta\beta}(r)$ is initially very large, but the heights of its peaks decay with increasing distance. This behavior of a pair-correlation function is a feature of configurations in which different atom species cluster together. The clustering of ''disordered'' atoms is most obvious from a direct visualization of the basal planes (Fig. 9).

In order to obtain an estimate of the average size of these clusters we adopt a measure first suggested by Abraham and co-workers[19] in studies of phase separation. Their approach is to calculate the value of r_{cluster} at which the partial $g(r)$ first equals 1 and use this as a measure of the average size of a cluster. Applying this criteria, it was found that the disordered regions decrease in size from 12 to 8 Å as the heat-treatment temperature is increased from 1000 to 2500 °C.

A comparison of the total $g(r)$ and the partial $g(r)$ from the ordered region for the v25 sample reveals that the peak heights are larger for the latter $g(r)$ indicating that the height of the total $g(r)$ is reduced by the existence of disordered regions. A comparison of the partial $g(r)$ of the ordered regions for both the v10 and v25 sample reveals that the broader $g(r)$ in the v10 sample is not only due to the increased size of the disorder regions but also the increased irregularity in the ordered regions.

CONCLUSION

The local order in glassy carbon was found to be similar to graphite for both samples, with the v10 sample, formed at a lower heat-treatment temperature, showing slightly more local disorder as indicated by the broader distribution of bond angles. This suggests a network model of glassy carbon in which local coordination is maintained and disorder arises from variations in bond length and bond angle, as is used to

describe silicate glasses. The increased broadness of the first peak in the $g(r)$ for the v10 sample and also in the distribution of bond angles supports this assertion. However, the observation of nonhexagonal rings suggests a change in the topology of glassy carbon from that of graphite that also needs to be accounted for. The main difference between the local structures of the two samples is not so much an increase in the degree of local disorder, as suggested by the bond-angle distributions, but the increased number of nonhexagonal rings in the v10 sample compared to the v25 sample, i.e., the main differences are topological rather than geometrical.

The existence of three- and four-membered rings in the simulated structures is an interesting result. This work can be regarded as complementary to *ab initio* simulations of amorphous carbon but only those in which the smaller rings appear as a necessary structural feature in order to create a three-dimensional model of glassy carbon consistent with the diffraction data.

Strong local curvature of the graphitic basal planes is a feature of both samples studied. This can be seen by a visualization of the simulated structures, the breadth of the basal planes, and the presence of nonhexagonal rings. The existence of the nonhexagonal rings is a direct consequence of the curvature of the basal planes, if sp^2 coordination is to be maintained. The larger number of nonhexagonal rings in the v10 sample and the increased breadth of the basal planes indicates that the v10 sample is more strongly buckled than the v25 sample. A general conclusion that can be made is that one effect on the structure of glassy carbon of annealing at a higher temperatures is to reduce the degree of buckling of the planes. The smaller height of the (002) peak in the v10 sample compared to the v25 sample is thus due to the increased buckling of the basal planes.

[1] G. M. Jenkins and K. Kawamura, *Polymeric Carbons-Carbon Fibre Glass and Char* (Cambridge University Press, Cambridge, 1976).
[2] C. A. Angell, J. Phys. Chem. Solids **49**, 863 (1988).
[3] R. L. McGreevy and L. Pusztai, Mol. Simul. **1**, 359 (1988).
[4] M. A. Howe, R. L. McGreevy, L. Pusztai, and I. Borzsak, Phys. Chem. Liq. **25**, 205 (1993).
[5] L. Pusztai and G. Toth, J. Chem. Phys. **94**, 3042 (1991).
[6] D. J. Tildesley and M. P. Allen, *Computer Simulation of Liquids* (Oxford Science, Oxford, 1987).
[7] D. G. McCulloch, S. Prawer, and A. Hoffman, Phys. Rev. B **50**, 5905 (1994).
[8] G. M. Jenkins and K. Kawamura, *Polymeric Carbons-Carbon Fibre Glass and Char* (Ref. 1), p. 67.
[9] O. Gereben and L. Pusztai, Phys. Rev. B **50**, 14 136 (1994).
[10] D. Cockayne, D. McKenzie and D. Muller, Microsc. Microanal. Microstruct. **2**, 359 (1991).
[11] D. Cockayne and D. McKenzie, Acta Crystallogr., Sect. A: Found. Crystallogr. **44**, 870 (1988).
[12] R. L. McGreevy, J. Phys.: Condens. Matter **3**, F9 (1991).
[13] D. S. Franzblau, Phys. Rev. B **44**, 4925 (1991).
[14] N. A. Marks, D. R. McKenzie, B. A. Pailthorpe, M. Bernasconi, and M. Parrinello, Phys. Rev. B **54**, 9703 (1996).
[15] C. Z. Wang and K. M. Ho, Phys. Rev. Lett. **71**, 1184 (1993).
[16] T. J. Lenosky, X. Gonze, M. Teter, and V. Elser, Nature (London) **355**, 333 (1992).
[17] S. J. Townsend, T. J. Lenosky, D. A. Muller, C. S. Nichols, and V. Elser, Phys. Rev. Lett. **69**, 921 (1992).
[18] G. Galli, R. M. Martin, R. Car, and M. Parrinello, Phys. Rev. Lett. **62**, 555 (1989).
[19] S. W. Kock, R. C. Desai, and F. F. Abraham, Phys. Rev. A **26**, 1015 (1982).